Narrow Long Josephson Junctions

Yu. Koval[#,*], A. Wallraff, M. Fistul, N. Thyssen[*], H. Kohlstedt[*] and A.V. Ustinov
Physikalisches Institut III, Universität Erlangen-Nürnberg, D-91058 Erlangen, Germany

***Abstract*—Long Josephson junctions of width down to less than 0.3 μm are fabricated using electron beam lithography. The junctions are made in niobium-aluminum-oxide trilayer technology using cross-linked PMMA for insulation. We measured the fluxon penetration field, the magnetic field period of the critical current modulation, and the Fiske step voltages of the junctions. A strong dependence of these quantities on the junction width is observed. Assuming a general-type relation between the spatial derivative of the phase and the spatial variation of the magnetic field along the plane of the junction, we derive a scaling relation between the measured quantities depending on the junction width. The derived relation is consistent with the experimental data.**

I. Introduction

Long Josephson junctions (LJJs), often also called Josephson transmission lines, display propagating fluxons and linear electromagnetic waves, which are used in various applications within superconductive electronics. These waves can be considered as quasi-one-dimensional, if the width w_1 of the junction (i.e. its dimension transverse to the direction of the wave propagation) is smaller than the Josephson penetration depth λ_J, which is typically of the order of several micrometers. This requirement sets an upper limit for w_1. By now there has been very little known about the lower limit for the width w_1. Usually, the natural limitation is imposed by the photolithographic preparation procedure which allows to produce junctions down to a few micrometers in width. However, the general direction of superconducting circuits development towards high frequencies and smaller dimensions rises a question of validity of the conventional one-dimensional LJJ model for sub-micrometer wide junctions. Another source of interest in making very narrow LJJs is the possibility of studying quantum effects in the Josephson fluxon dynamics. Quantum features of fluxons should be observable in a parameter range where the Josephson coupling energy and/or the energy of the fluxon's screening currents are comparable with the charging energy of the junction, and the temperature is low enough. New physical phenomena were predicted for quantum fluxons [1], [2] but no experimental studies of them have been reported until now.

We investigate the properties of ultra-narrow high quality junctions with gradually decreasing width. We find that already classic dynamics of Josephson fluxons changes in the sub-micrometer range. In Sec. II our fabrication procedure for sub-micron-wide LJJs is elaborated. The measurements are described in Sec. III. A theoretical approach to explain the width dependence of the measured junction characteristics is presented in Sec. IV. In Sec. V we discuss the effect of the electromagnetic window around the junction on the Fiske step voltages, as a special case of our theoretical model. Sec. VI contains concluding remarks.

II. Samples

The fabrication of high quality LJJs should satisfy the following demands. The process should allow to vary the junction width from several micrometers down to the sub-micrometer range of about 0.1 μm. At the same time, the junction width has to remain constant over the junction length $L \gg \lambda_J$, typically about several hundreds of micrometers. The junctions should have small spread in critical current density over the whole wafer. Moreover, the overlap of the bottom and top electrodes near the junction area has to be as small as possible to avoid the influence of this passive region on the junction properties [3].

The most reliable and established way to fabricate high quality long junctions with a small spread of critical current density across the whole waver is based on the Nb/Al-AlO_x/Nb trilayer process. The use of Nb allows to perform measurements at 4.2 K, which significantly simplifies experiments as in comparison with all-Al junctions.

Several different approaches do exist for Josephson junction preparation using a trilayer. The major differences between the processes are in the formation of the junction lateral dimensions and in the method of electrode insulation. In the so called SNAP (selective niobium anodization process) technology, a single step anodic oxidization is the process which reaches both goals [4]. However, this process is not suitable for sub-micron junctions [5]. Junctions with dimensions of less than 1 μm are usu-

Institute of Microelectronics Technology, RAS, Chernogolovka, 142432, Russia.
* ISI, Forschungszentrum Jülich GmbH, 52425 Jülich, Germany.
Manuscript received September 15, 1998.
A. Wallraff, +49 – (0)9131 – 857120, fax +49 – (0)9131 – 15249, http://www.physik.uni-erlangen.de/pi3/ustinov/, wallraff@physik.uni-erlangen.de.

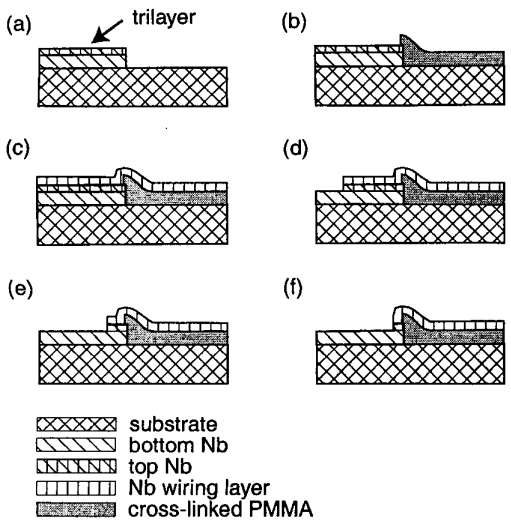

Fig. 1. Schematic diagram of fabrication procedure. (a) formation of a straight edge in the trilayer, (b) insulation of the trilayer edge, (c) deposition of the Nb wiring, (d) removal of Nb wiring and top Nb from all areas except the area of junction, (e,f) narrowing of junction by electron beam lithography and RIE.

ally produced by reactive ion etching (RIE) and dielectric layer deposition. Sometimes this technology is termed SNIP (selective niobium insulation process) [6]. In this process the same resist mask can be used for both etching and dielectric layer deposition [7]–[9], which provides a self-alignment effect. Though such a process is suitable for our task, it does not satisfy the demand of having a small passive region for sub-micron junctions.

We developed a modified approach for long junction preparation. It is based on the use of highly cross-linked polymethylmethacrylate (PMMA) for insulation. It is well known that, under high electron exposure dose, the positive electron resist PMMA turns to negative. Exposed areas become insoluble in strong solvents and are very thermostable and adhesive [10]. These features make highly cross-linked PMMA compatible with a number of technological processes which do not require heating above approximately 200° C. It is possible to use electron beam lithography, making use of back-scattered electrons, to achieve highly cross-linked PMMA adjoining the trilayer and simultaneously covering only its edge without an overhang. The absence of insulator overhang is the key feature to avoid overlap of Nb electrodes outside of the junction area. Therefore, self-alignment of cross-linked PMMA is a feasible method of edge insulation.

A. Fabrication Steps

The Nb/Al-AlO_x/Nb trilayer was deposited by magnetron sputtering onto a thermally oxidized silicon wafer. The thickness of the bottom and top Nb electrodes are about 100 nm and 50 nm, respectively. The critical current density is approximately 200 A/cm^2. Schematically, the process of LJJ preparation is shown in Fig. 1.

The planar trilayer geometry was formed by photolithography and SF_6 RIE (Fig. 1a). Then one edge of the structure was defined by electron beam lithography and SF_6 RIE and the edge was covered by cross-linked PMMA 950 K (Fig. 1b). To carry out this step, a 1 μm wide strip was exposed along the whole length of the junction to be formed. The distance between the edge of the exposed strip and the edge of the trilayer was about 0.3 μm (Fig. 2). This distance was sufficient to avoid an exposure of the PMMA on top of the trilayer due to small misalignment, stage drift or other effects. As shown in Fig. 2, the area adjoint to the exposed line is affected by the electrons which are back scattered from the substrate. Due to the difference in the atomic numbers and densities of Nb and SiO_2, the back-scattered electrons are stopped by the trilayer and protect the PMMA on it. This effect provides self-alignment of the insulator edge because the border of the cross-linked PMMA is determined by the trilayer edge. In order to use this effect, only the parameters of electron beam exposure need to be determined correctly.

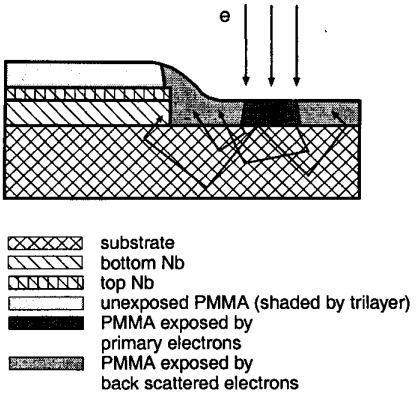

Fig. 2. Self-alignment of cross-linked PMMA to the trilayer edge. Electrons back scattered from the substrate expose the resist far from the region of primary electron irradiation. But the PMMA on the top of the trilayer is protected by Nb and the PMMA on the edge is half protected due to the shadow effect.

To optimize the exposure, we tried irradiation with 4, 10, and 20 keV electrons and doses of 1 – 100 mC/cm^2. After exposure the samples were developed in acetone for 5 minutes. Development in acetone removes all resist except for the cross-linked regions. After edge insulation a Nb wiring layer of 100 nm thickness was deposited (Fig. 1c). Contact pads and junction area were formed by photolithography and RIE. Up to this step we have fabricated long junctions of 10 – 20 μm width. These junctions were tested and later used for a subsequent decrease of their width. The width of the junctions was decreased in several steps using electron beam lithography and RIE, as shown in Fig. 1d,e & f.

B. Determination of Electron Dose

To determine the dose of exposure required to cover the edge of the trilayer, we measured the dependence of the exposed strip width on the dose for 4, 10 and 20 keV electrons. In the experiments we used thermally oxidized

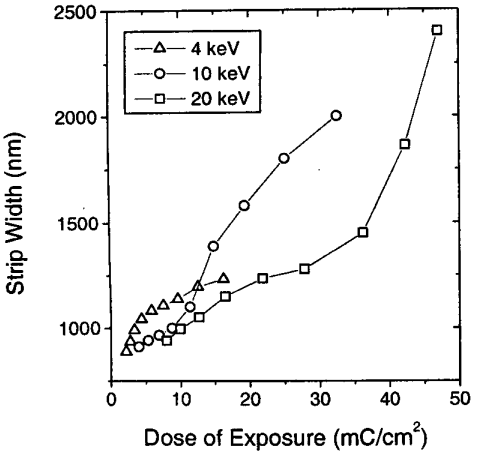

Fig. 3. Experimental dependence of cross-linked PMMA strip width on dose of electron exposure for 4, 10 and 20 keV electron energy.

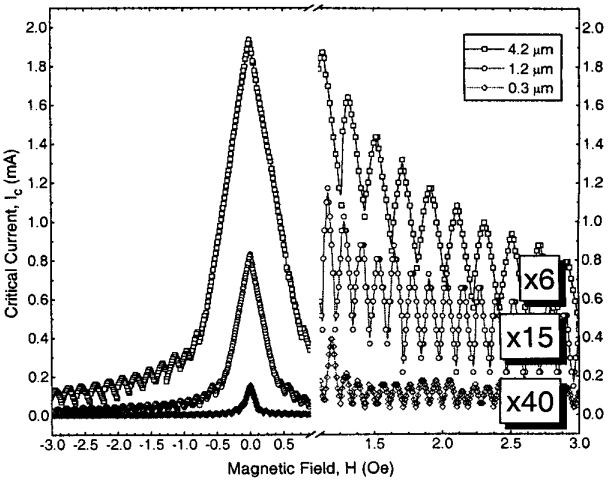

Fig. 4. Critical current modulation $I_c(H)$ with magnetic field. In the range $H = 1 \ldots 3$ Oe the critical currents are multiplied by a constant factor for better visibility of the high field modulation period. The multiplication factor is quoted in the box atop of each curve.

Si and PMMA 950 K. The initial width of an exposed strip was 1 μm. The results of the measurements are shown in Fig. 3. These curves allow to determine the dose needed in dependence on the electron energy and wanted strip width. In our case the distance between trilayer edge and exposed strip edge is 300 nm, so the width of the strip should increase by 600 nm due to the back-scattered electrons. It is clearly seen that for 4 keV electrons this goal can hardly be reached. For 10 keV we find an optimal dose of 20 mC/cm^2 and for 20 keV of 40 mC/cm^2.

It is obvious that the determined value is the minimum dose at which the cross-linked PMMA approaches the edge of the trilayer. We found reliable edge insulation of the trilayer at about twice this dose. The resist out of the area of primary exposure is influenced by the electrons from all directions, due to the nearly cosine angle distribution of the back-scattered electrons. Near the edge of the trilayer, we observe a shielding of the back-scattered electrons because of their absorption in Nb, which leads to a shadow effect on the resist. To acquire more precise values, we additionally investigated the covering of the trilayer edge by resist. We found that the estimations made are in very good agreement with the obtained results. For 10 keV electrons a good edge covering with a small overhang of resist was obtained for a dose of ~ 40 mC/cm^2. For 20 keV we got the best dose of approximately $60-70$ mC/cm^2. The shadow effect is reduced for the higher energetic 20 keV electrons.

For junction preparation both 10 keV, 40 mC/cm^2 and 20 keV, 65 mC/cm^2 regimes were used and no influence of the selected regimes on the junction properties was found. It is worth to note that cross-linked PMMA does not degrade due to multiple thermal cycling from room temperature down to 4.2 K.

III. Junction Characteristics

In this section we present the data acquired for ten 200 μm long junctions of different width w_1 varied between 4.2 μm and 0.3 μm. All junctions were measured at $T = 4.2$ K. A magnetic field H of up to 40 Oe could be applied in the plane of the junction perpendicular to its long dimension. Residual magnetic fields were screened by a cryoperm shield.

First, the current voltage characteristics (IVCs) have been acquired. All junctions are high quality with a large subgap resistance R_{sg}. The actual widths of the junctions have been determined by comparison of their normal resistance R_n with the R_n of a 4.2 μm wide reference junction. The width of the reference junction was determined using a scanning electron microscope (SEM). The Josephson penetration depth was estimated to about 25 μm.

A. Magnetic Field Patterns

The homogeneity of all junctions was tested by measuring the modulation pattern of the critical current I_c versus H. In Fig. 4 the patterns of three samples of width $w_1 = 4.2$, 1.5 and 0.3 μm are shown. $I_c(0)$ scales as expected due to the different widths of the junctions. Very remarkable is a strong dependence of the fluxon penetration field H_{c_1} and the field modulation period ΔH on w_1. For junctions for which $\lambda_L \ll w_1 < \lambda_J$ it is usually assumed that the magnetic field at which fluxons can penetrate into a LJJ is given by $H_{c_1} = \Phi_0/\pi\lambda_J\Lambda$, where Λ is the magnetic field penetration depth depending only on the film thicknesses ($\Lambda \approx 2\lambda_L$ for thick electrodes) and Φ_0 is the magnetic flux quantum. Therefore, H_{c_1} should be independent of w_1 in this case. Similarly, the modulation of I_c at high fields should have a period given by $\Delta H = \Phi_0/L\Lambda$. The period ΔH corresponds to the subsequent penetration of additional flux quanta into the LJJ, which also should be independent of w_1.

Obviously, our experimental results are not width independent. From the data we conclude that the magnetic

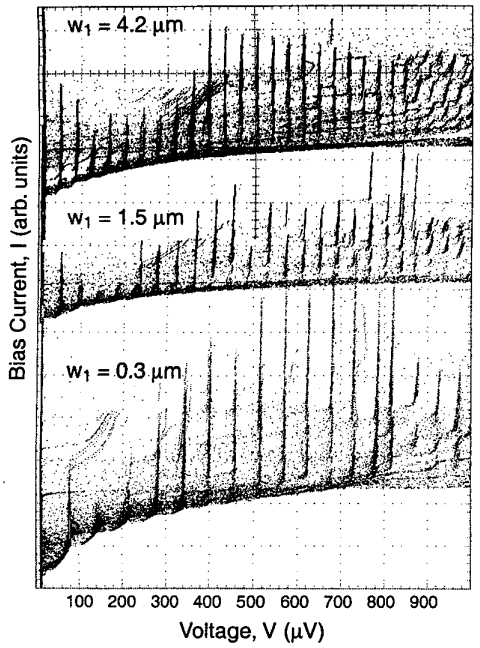

Fig. 5. Superimposed traces of Fiske resonances for $H = 0 \ldots 40$ Oe. The Fiske step families for junctions of width $w = 4.2$, 1.5 and 0.3 μm are shown.

field penetrates deeper into the more narrow junctions than into the wider ones, thus decreasing the values of H_{c_1} and ΔH. In Sec. IV we present a model which explains our experimental data by taking into account the width dependent penetration of the magnetic field into the electrodes.

B. Fiske Steps

Fiske steps (FSs) have been measured in all junctions by tracing the IVCs during a continuous sweep of the external magnetic field in the range between $H = 0 \ldots 40$ Oe. These IVCs are superimposed using a digital storage oscilloscope, such that the FSs can be clearly resolved. In Fig. 5, the superimposed IVCs are plotted for the same junctions as shown in Fig. 4. An increase of the FS voltage spacing with decreasing junction width is observed. This indicates an increase of the velocity of electromagnetic waves (i.e. the Swihart velocity $\bar{c}$) in the junction. The dependence of the Fiske step voltages on the width of the junction is discussed below in Sec. IV.

IV. Model

For not too narrow long Josephson junctions, their dynamic and static properties can be well explained by the perturbed sine-Gordon model. This model can be modified in order to qualitatively include a width dependence into the equation. Our approach is based on the modification of the magnetic field penetration into the electrodes along the (shorter) y-dimension. x is the coordinate along the longer dimension of the junction. We introduce the width dependent factor $\alpha(y)$ into the usual relation between the Josephson phase difference $\varphi(x, y)$ and the magnetic field $H(x, y)$

$$\frac{d\varphi(x,y)}{dx}\alpha(y) = \frac{H_y(x,y)d'}{\Phi_0} \ , \ \frac{d\varphi(x,y)}{dy}\alpha(y) = \frac{H_x(x,y)d'}{\Phi_0} \ . \tag{1}$$

This effectively introduces a width dependence of the magnetic thickness d', which accounts for the larger field penetration into a narrow junction. Using this assumption we can write down a 2D sine–Gordon equation of the following form

$$\frac{\partial^2\varphi}{\partial x^2} + \frac{\partial^2\varphi}{\partial y^2} - \frac{1}{\bar{c}^2\alpha(y)}\frac{\partial^2\varphi}{\partial t^2} + \frac{1}{\lambda_J^2\alpha(y)}\sin(\varphi) = 0 \ . \tag{2}$$

Using (2) we can immediately extract the modified Swihart velocity $\tilde{c}(w) = \bar{c}(\infty)\sqrt{\alpha(y)}$ and the Josephson length $\tilde{\lambda}_J(w) = \lambda_J(\infty)\sqrt{\alpha(y)}$. Similarly, we have to change the relation between H and φ on the boundaries

$$\frac{d\varphi(0,y)}{dx} = \frac{d\varphi(L,y)}{dx} = \frac{Hd'}{\Phi_0}\alpha(y) \ . \tag{3}$$

From (3) we find the modified magnetic field $\tilde{H}(w) = \tilde{H}(\infty)\alpha(y)$. Using these relations, one can find the dependencies of the measured quantities on the width-dependent parameter $\alpha(y)$

$$\tilde{c} \ \propto \ \sqrt{\alpha(y)} \ , \tag{4}$$

$$\tilde{H}_{c1} \ \propto \ \frac{1}{\alpha(y)^{3/2}} \ , \tag{5}$$

$$\Delta\tilde{H} \ \propto \ \frac{1}{\alpha(y)} \ . \tag{6}$$

Assuming a self-consistent dependence of these three quantities on $\alpha(y)$, we can write down the following scaling relation between them

$$\tilde{c} \propto \frac{1}{\tilde{H}_{c1}^{1/3}} \propto \frac{1}{\sqrt{\Delta\tilde{H}}} \ . \tag{7}$$

By analyzing the experimental data according to (7), we can expect a linear scaling of the three expressions (7). This scaling relation is plotted in Fig. 6 using the data measured for all ten junctions. Apparently, a good qualitative agreement between the data and the model can be found. We chose to plot the magnetic parameters versus the Fiske step voltage, because the latter is measured most accurately in experiment. The magnetic parameters are supposed to be influenced stronger by the critical current density inhomogeneities and parasitic flux in the superconducting films. These reasons may also explain scattering of the data around the linear fit.

V. Discussion

Our theoretical model, described in the previous section, qualitatively explains both the static and the dynamic properties of our junctions with good accuracy. Alternatively, the dynamic properties can also be explained

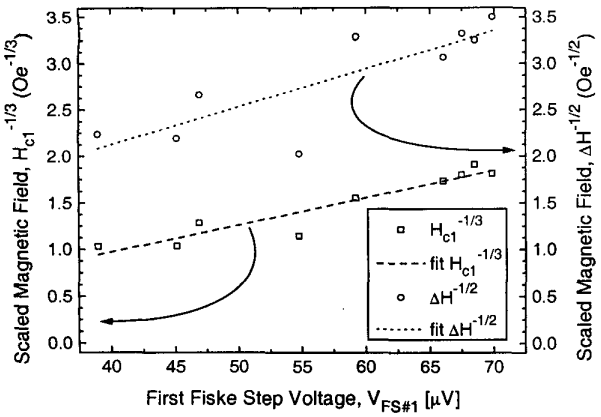

Fig. 6. The scaling relation (7) between magnetic fields H_{c1} and ΔH and the first Fiske step voltage $V_{FS\#1}$. Linear fits are shown by dashed lines.

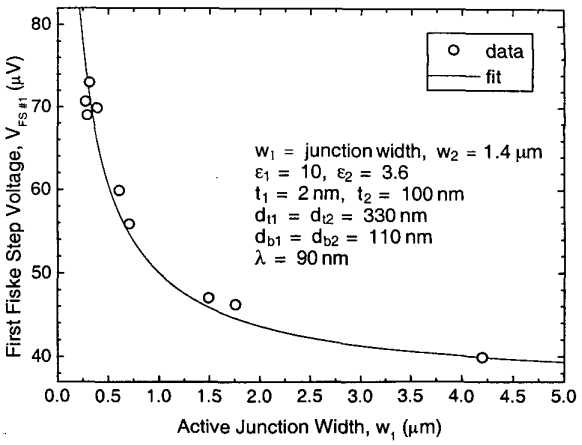

Fig. 7. Fit of width dependence of the maximum first Fiske step voltage $V_{FS\#1}$ according to (8). The values of the fixed parameters and the fitting parameter are quoted in the inset.

by a model first developed by Lee and Barfknecht in [11], [12]. There, the variation of the Fiske step voltage spacing with junction width w_1 is explained by taking into account the change of the velocity of light $\bar{c}$ in the bare junction due to the passive region formed by the overlapping electrodes (i.e. the electromagnetic window surrounding the junction area). This treatment is compatible with our model in the sense that it describes a special case of (2), where the Swihart velocity is modified due to an effective passive region, neglecting magnetic field penetration effects. Lee et al. derived a formula for the modified Swihart velocity

$$\tilde{c} = c \left(\frac{\frac{w_1 \epsilon_1}{t_1} + \frac{w_2 \epsilon_2}{t_2}}{\frac{w_1}{d_1'} + \frac{w_2}{d_2'}} \right)^{-1/2}, \qquad (8)$$

where c is the velocity of light in vacuum, $w_{1,2}$ is the width of active and passive region, respectively, $t_{1,2}$ and $\epsilon_{1,2}$ are the thicknesses and the dielectric constants of the respective regions, and $d'_{1,2}$ is the magnetic thickness of the barrier. With $\epsilon_1 = 10$ for the AlO_x barrier, $\epsilon_2 = 3.6$ for the PMMA in the passive region and the film thicknesses determined during sample preparation, one can fit the width dependence of the maximum Fiske step voltages $V_{FS\#1}$ using (8) and w_2 as a fit parameter. Good agreement can be achieved assuming an effective $w_2 = 1.4\,\mu$m (see Fig. 7). We note, however, that the real width w_2 of the window region in our junctions was smaller than $0.2\,\mu$m. Therefore the explanation based on (8) is not entirely consistent with our experimental data. Moreover, that approach does not explain the modification of the magnetic field penetration into narrow junctions as indicated by our measurements of H_{c_1} and ΔH.

VI. Conclusion

High quality narrow long Josephson junctions show a strong dependence of the junction characteristic parameters on the junction width. The data are described in a consistent way by considering a general-type width dependence of the phase gradient on the magnetic field. We have shown, that junction electrodynamics and static properties are strongly modified in long junctions which are more narrow than the Josephson penetration depth λ_J but wider than the London penetration depth λ_L. These effects have to be taken into account, if fluxon dynamics in narrow long Josephson junctions is investigated in the nonlocal or in the quantum regime.

References

[1] T. Kato and M. Imada, *J. Phys. Soc. Jpn.*, vol. 65, no. 9, p. 2963, 1996.

[2] A. Shnirman, E. Ben-Jacob, and B. Malomed, *Phys. Rev. B*, vol. 56, no. 22, p. 14677, 1997.

[3] N. Thyssen, A. V. Ustinov, H. Kohlstedt, S. Pagano, J. G. Caputo, and N. Flyzantis, *IEEE Trans. Appl. Supercond.*, vol. 5, p. 2965, 1995.

[4] H. Kroger, L. H. Smith, and D.W. Jillie, *Appl.Phys.Lett*, vol. 39, p. 280, 1981.

[5] T. Imamura and S. Hasuo, *J. Appl. Phys.*, vol. 64, no. 3, p. 1586, 1988.

[6] S. Morohashi, F. Shinoki, A. Shoji, M. Aoyagi, and H. Hayakawa, *Appl. Phys. Lett.*, vol. 46, p. 1179, 1985.

[7] H. G. LeDuc, A. Judas, S. R. Sypher, B. Bumble, B.D. Hunt, and L.A. Stern, *IEEE Trans. Mag.*, vol. 27, no. 2, p. 3192, 1991.

[8] A. W. Lichtenberger, D. M. Lea, C. Li, F. L. Lloyd, F. L. Feldmann, R. J. Mattauch, S.-K. Pan, and A.R. Kerr, *IEEE Trans. Magn.*, vol. 27, no. 2, p. 3168, 1991.

[9] V. P. Koshelets, S. A. Kovtonyuk, I. L. Serpuchenko, L. V. Filipenko, and A. V. Shchukin, *IEEE Trans. Magn.*, vol. 27, no. 2, p. 3141, 1991.

[10] Y. Koval, T. Borzenko, and V. Kudryshov, *Microelektronika*, vol. 24, no. 6, p. 460, 1995.

[11] G.S. Lee, *IEEE Trans. Appl. Supercond.*, vol. 1, no. 3, p. 121, 1991.

[12] G.S. Lee and A.T. Barfknecht, *IEEE Trans. Appl. Supercond.*, vol. 2, no. 2, p. 67, 1992.